JOURNAL OF COMPUTATIONAL PHYSICS **147,** 166–186 (1998)
ARTICLE NO. CP986087

Numerical Algorithms for the Direct Spectral Transform with Applications to Nonlinear Schrödinger Type Systems

S. Burtsev,*[,1] R. Camassa,* and I. Timofeyev†[,2]

**Theoretical Division and Center for Nonlinear Studies, Los Alamos National Laboratory, Los Alamos, New Mexico 87545; †Department of Mathematical Sciences, RPI, Troy, New York 12180-3590*
E-mail: roberto@cnls.lanl.gov, timofi@rpi.edu

Received March 11, 1998; revised August 14, 1998

We implement two different algorithms for computing numerically the direct Zakharov–Shabat eigenvalue problem on the infinite line. The first algorithm replaces the potential in the eigenvalue problem by a piecewise-constant approximation, which allows one to solve analytically the corresponding ordinary differential equation. The resulting algorithm is of second order in the step size. The second algorithm uses the fourth-order Runge–Kutta method. We test and compare the performance of these two algorithms on three exactly solvable potentials. We find that even though the Runge–Kutta method is of higher order, this extra accuracy can be lost because of the additional dependence of its numerical error on the eigenvalue. This limits the usefulness of the Runge–Kutta algorithm to a region inside the unit circle around the origin in the complex plane of the eigenvalues. For the computation of the continuous spectrum density, this limitation is particularly severe, as revealed by the spectral decomposition of the L^2-norm of a solution to the nonlinear Schrödinger equation. We show that no such limitations exist for the piecewise-constant algorithm. In particular, this scheme converges uniformly for both continuous and discrete spectrum components.

Key Words: nonlinear Schrödinger equation; Zakharov–Shabat eigenvalue problem; nonlinear optics.

1. INTRODUCTION

The discovery and development of the soliton theory [1, 2] has had deep repercussions in physics and applied mathematics. This theory has made possible the explicit integration

[1] Present address: Corning Inc., Corning, NY 14831.

[2] To whom correspondence should be addressed at present address: Courant Institute of Mathematical Sciences, 251 Mercer Street, New York, New York 10012. E-mail: ilyat@cims.nyu.edu.

0021-9991/98 $25.00

of several partial differential equations (PDEs) with universal applicability. In particular, these equations were linearized via an associated linear system, the Lax pair, and explicitly integrated in the following sense: First, rich classes of exact solutions, infinite hierarchies of conservation laws, and infinite-dimensional analogs of the action-angle variables were derived. Second, the solution of the Cauchy problem on the infinite line was recast in the form of a solvable linear integral equation, and the asymptotic nature of its solutions was determined explicitly.

Two main ingredients in the solution of the Cauchy problem for integrable nonlinear partial differential equations are the direct spectral transform and its inverse counterpart. These are nonlinear analogs of the direct and inverse Fourier transforms, respectively. They both involve a single linear system of ordinary differential equations with a free (spectral) parameter and, in general, are not tractable analytically. Hence, in order to solve them, one has to resort to numerical solvers.

Simple and effective PDE-solvers, developed in recent years, have made the numerical study of nonlinear wave phenomena in one spatial dimension relatively straightforward. Nevertheless, "raw" numerical modeling is still prohibitively time-consuming when one has to map out multidimensional parameter spaces. Moreover, even an accurate and comprehensive numerical simulation stops short of providing a fundamental understanding of any nonlinear wave phenomenon.

In the special case of near-integrable partial differential equations, fundamental understanding can be provided by decomposing the wave field into "normal" coordinates, i.e., the soliton and nonsoliton components, also termed as the nonlinear spectral data. Such a decomposition can be readily achieved by inserting the numerical solution of a given near-integrable partial differential equation into a direct spectral transform solver. Apart from its intrinsic value, this decomposition can be useful for verifying and complementing perturbation calculations that describe the "flow" of the spectral data. To do this one has to analyze snapshots of the potential for different times. These and other reasons (see [3]) necessitate the development of efficient high-quality numerical solvers for the direct spectral transform.

In this paper we concentrate on the nonlinear Schrödinger (NLS) equation

$$iq_z + \frac{1}{2}q_{tt} + q^*q^2 = P, \tag{1}$$

which describes propagation of light pulses in an optical fiber with the anomalous[1] group-velocity dispersion [4, 5]. Here, we prefer to use the optical notation in which the normalized time t plays the role of a spatial coordinate and the normalized distance z plays the role of a time-like coordinate, while $q(t, z)$ is the complex envelope of the electric field. The perturbation P is specified by the particular physical problem at hand. When $P = 0$, the NLS system is integrable. The linearization of the NLS system is achieved by recasting this system as the Zakharov–Shabat spectral problem [6], which is a system of two ODEs for

[1] The case of normal group-velocity dispersion leads to a similar equation with only a change of the relative signs of the terms on the left-hand side of (1). In this case the associated spectral problem is self-adjoint and, hence, somewhat simpler to treat.

the scalar wave functions ϕ_1 and ϕ_2,

$$\begin{aligned} \frac{d\phi_1}{dt} &= q\phi_2 - i\zeta\phi_1, \\ \frac{d\phi_2}{dt} &= -q^*\phi_1 + i\zeta\phi_2, \end{aligned} \tag{2}$$

where ζ is an eigenvalue parameter. By using the Zakharov–Shabat spectral problem, in combination with the appropriately chosen linear ODEs which define the z-evolution of ϕ_1 and ϕ_2, one can also solve analytically several other important nonlinear partial differential equations. Besides the nonlinear Schrödinger equation, which is currently receiving a great deal of attention due to its technological applications in fiber optics, these partial differential equations include the Maxwell–Bloch system, the sine–Gordon equation, the usual and the modified Korteveg–de Vries equations, etc.

In this paper, we present an efficient numerical algorithm for solving the direct Zakharov–Shabat spectral problem. We have incorporated this numerical algorithm in a code that computes the flow of the spectral data and in particular eigenvalues, for the perturbed NLS equation (1). For this application, we optimize the performance of the eigenvalue-search algorithm by using our knowledge of the history of the spectral data. Our code is able to speed up the search for each eigenvalue in subsequent snapshots of the perturbed NLS solution by a factor of 5, provided that the number of eigenvalues does not change from one snapshot of the solution to another.

The main focus of this work is to describe and compare two different algorithms for solving Zakharov–Shabat spectral problem, which differ by how one solves the system of ordinary differential equations (2) with ζ as a parameter. The first approach [3] replaces the potential q with its piecewise-constant approximation. This allows us to solve the corresponding ODE analytically. The second approach [7] proposes using a high-order ODE integrator, such as a fourth-order Runge–Kutta scheme. Both algorithms use a grid-search approach to find the eigenvalues. We have tested both methods on a variety of explicitly solvable potentials: soliton, oversoliton, and a rectangular potential. One of the most important findings that emerges from our study is that only the piecewise-constant algorithm is effective computing the continuous spectrum contribution to the L^2-norm (the conserved "number of particles" functional) of solutions of the unperturbed NLS equation.

The numerical error in the Runge–Kutta approach cannot be controlled uniformly over the spectrum. Specifically, the Runge–Kutta's local truncation error depends on the eigenvalue as ζ^4, which limits its applicability to the unit circle region around the origin of the complex ζ plane. This limitation is dramatically revealed by the spectral decomposition of the L^2-norm of solutions of the NLS equation. Our tests show that for a given discretization step the error in computing the continuous spectrum contribution to the L^2-norm by the Runge–Kutta method can be over an order of magnitude larger than the error of the piecewise-constant method.

The layout of this paper is the following. In Section 2, we recall a few basics of the soliton theory. The properties of the spectral problem depend heavily on the type of boundary conditions, i.e., an infinite-line problem with the potential $q(t)$ decaying at infinity or a t-periodic problem for the potential $q(t)$. In this paper we only investigate the infinite line problem. In Section 3, we introduce both solvers: Runge–Kutta and piecewise-constant, and describe our implementation of the eigenvalue-search algorithm. In Section 4, we

present the results of the error analysis. The test results are given in Section 5. Finally, in Section 6, we illustrate the performance of the eigenvalue solver, based on a piecewise-constant approximation and the eigenvalue search algorithm by applying it to a realistic fiber-optic problem: *Non-return-to-zero* to soliton data conversion in the optical line with sliding frequency guiding filters [8, 9].

2. THE DIRECT AND INVERSE SPECTRAL TRANSFORMS

When the perturbation P is absent, Eq. (1) is equivalent to the overdetermined linear system for a vector-valued wave function $\mathbf{\Phi} = (\phi_1, \phi_2)^{\mathrm{T}}$ (with $(\cdot, \cdot)^{\mathrm{T}}$ denoting the transpose),

$$\mathbf{\Phi}_t + U\mathbf{\Phi} = 0, \tag{3}$$

$$\mathbf{\Phi}_z + V\mathbf{\Phi} = 0, \tag{4}$$

where 2×2 matrix functions U and V and the two-dimensional (column) vector function $\mathbf{\Phi}$ depend on the time t, the coordinate z, and the spectral parameter ζ in the following fashion:

$$U = i\zeta\sigma_3 + u,$$
$$V = i\zeta^2\sigma_3 + \zeta u + v - i\zeta^2 I.$$

Here,

$$\sigma_3 = \begin{pmatrix} 1 & 0 \\ 0 & -1 \end{pmatrix}, \quad I = \begin{pmatrix} 1 & 0 \\ 0 & 1 \end{pmatrix},$$
$$u = \begin{pmatrix} 0 & -q \\ q^* & 0 \end{pmatrix}, \quad v = \frac{i}{2}\begin{pmatrix} -|q|^2 & -q_t \\ -q_t^* & |q|^2 \end{pmatrix}.$$

The function $q(t, z)$ is the wave field of the unperturbed NLS equation, and the system (3) is nothing but the scalar system (2) rewritten in a vector form. The compatibility condition $U_z - V_t + VU - UV = 0$ between Eqs. (3) and (4) is exactly the unperturbed NLS system.

Let us recall a few properties of the system pair (3) and (4). Equation (3) has the structure of an eigenvalue problem with the complex parameter ζ (the Zakharov–Shabat spectral problem [6]). This problem can be thought of as a nonlinear analog of the Fourier transform for linear problems. Generically, an initial condition $q(t, 0)$ gives rise to a continuous spectrum represented by a function $r(\zeta)$, with each real-valued ζ being the analog of the frequency of a dispersive wave component. In addition to the continuous spectrum, the Zakharov–Shabat spectral problem supports a discrete spectrum, whose corresponding modes have no counterpart in the Fourier transform. This discrete spectrum consists of complex pairs $\{\zeta_k = \xi_k + i\eta_k, \rho_k\}$, $k = 1, \ldots, N$, where N is the number of solitons which will emerge from the initial data for sufficiently large z. The properties of these solitons are determined by ζ_k and ρ_k as follows: for each k, the real part of the complex eigenvalue ζ_k, $\xi_k = \mathrm{Re}(\zeta_k)$ equals one half of the corresponding soliton frequency, and the imaginary part $\eta_k = \mathrm{Im}(\zeta_k)$ equals one half of the soliton amplitude; the complex coefficient ρ_k parameterizes the soliton's initial position and its complex phase. In the limit of infinitely small q, the discrete spectrum is absent and the continuous spectrum coincides with the spectral density of linear Fourier harmonics.

To present the *Spectral Data* $= \{r(\zeta), \zeta \in R; \zeta_k, \rho_k, k = 1, N\}$ in greater detail, we need to recall a few extra elements of the Zakharov–Shabat spectral problem. We begin with the continuous spectrum, represented by the function $r(\zeta)$ when the eigenvalue ζ is located on the real axis. First, we introduce the vector solutions $\mathbf{\Phi}_1$ and $\mathbf{\Phi}_2$ (the Jost functions) of systems (3) and (4),

$$\begin{aligned} \mathbf{\Phi}_1 &= \begin{pmatrix} 1 \\ 0 \end{pmatrix} \exp(-i\zeta t)[1 + o(1)], \quad t \to -\infty, \\ \mathbf{\Phi}_2 &= \begin{pmatrix} 0 \\ -1 \end{pmatrix} \exp(i\zeta t)[1 + o(1)], \quad t \to -\infty, \end{aligned} \tag{5}$$

fixed by their asymptotics at the left end $t \to -\infty$. Hence, for each point ζ of the continuous spectrum one finds two independent solutions $\mathbf{\Phi}_{1,2}$. We also need the solutions $\mathbf{\Psi}_1$ and $\mathbf{\Psi}_2$ fixed by their asymptotics at the right end,

$$\begin{aligned} \mathbf{\Psi}_1 &= \begin{pmatrix} 1 \\ 0 \end{pmatrix} \exp(-i\zeta t)[1 + o(1)], \quad t \to \infty, \\ \mathbf{\Psi}_2 &= \begin{pmatrix} 0 \\ 1 \end{pmatrix} \exp(i\zeta t)[1 + o(1)], \qquad t \to \infty. \end{aligned} \tag{6}$$

Out of these vector solutions $\mathbf{\Phi}_{1,2}$ and $\mathbf{\Psi}_{1,2}$, one can construct two different fundamental matrix solutions $\Phi = (\mathbf{\Phi}_1, \mathbf{\Phi}_2)$ and $\Psi = (\mathbf{\Psi}_1, \mathbf{\Psi}_2)$ which are related to each other via a scattering matrix S

$$\Phi = \Psi S, \quad S = \begin{pmatrix} a & b^* \\ b & -a^* \end{pmatrix}. \tag{7}$$

The function $r(\zeta)$ is the ratio of the elements of the scattering matrix S: $r(\zeta) = b(\zeta)/a(\zeta)$. By using the relation (7), one derives useful formulas which are valid for real values of the spectral parameter ζ,

$$\begin{aligned} a(\zeta) &= \lim_{t\to\infty} \phi_1(t, \zeta) \exp(i\zeta t), \\ b(\zeta) &= \lim_{t\to\infty} \phi_2(t, \zeta) \exp(-i\zeta t), \end{aligned} \tag{8}$$

where the scalar functions $\phi_{1,2}$ are the components of the vector-valued Jost function $\mathbf{\Phi}_1$.

Due to the fact that the Zakharov–Shabat spectral problem is not self-adjoint, the corresponding eigenvalues ζ_k are complex-valued. Each eigenvalue is located in the upper half ζ-plane, and its corresponding Jost function is fixed by its asymptotics at the left end,

$$\mathbf{\Phi}_{1k} = \begin{pmatrix} 1 \\ 0 \end{pmatrix} \exp(-i\zeta_k t)[1 + o(1)], \quad t \to -\infty.$$

The asymptotics of the Jost function $\mathbf{\Phi}_{1k}$ on the right end is parameterized by normalization constant b_k,

$$\mathbf{\Phi}_{1k} = b_k \begin{pmatrix} 0 \\ 1 \end{pmatrix} \exp(i\zeta_k t)[1 + o(1)], \quad t \to \infty.$$

The coefficient ρ_k is expressed in terms of b_k and ζ-derivative a'_k of the spectral coefficient a at the position of the eigenvalue ζ_k: $\rho_k = b_k/a'_k$. We assume that a potential $q(t)$ is sufficiently smooth and that it vanishes at $|t| \to \infty$ fast enough so that the discrete spectrum contains a finite number of eigenvalues. We also assume that each zero of a is a simple one. The mapping $q(t) \to$ *Spectral Data* makes up the direct spectral problem. The solution of the inverse mapping may be reduced to a linear integral equation of Volterra type (Gelfand–Levitan–Marchenko system) [1, 2].

For the unperturbed NLS equation the evolution of the spectral data in z can be computed using Eq. (4). By substituting the evolved spectral data into the Gelfand–Levitan–Marchenko system one can determine the solution $q(t, z)$ at any $z > 0$. The essential point that makes this procedure possible is that the spectral data evolve in z in a trivial manner for any initial function $q(t, 0)$:

$$\begin{aligned} d\zeta_k/dz &= 0, \\ d\rho_k/dz &= 2i\zeta_k^2\rho_k, \\ dr(\zeta, z)/dz &= 2i\zeta^2 r. \end{aligned}$$

For instance, in the case of an initial condition with discrete spectrum only ($r(\zeta) = 0$), one can write down an explicit solution that describes N interacting solitons. In the simplest case of a single soliton, $N = 1$, we have a familiar sech-shaped pulse:

$$\begin{aligned} q_s &= \frac{2\eta e^{i\phi}}{\cosh(2\eta\theta)}, \\ \theta &= t + 2\xi z - t_0, \\ \phi &= -2\xi(t + 2\xi z) + 2i(\eta^2 + \xi^2)z + \phi_0, \end{aligned} \tag{9}$$

$$2\eta t_0 = \ln[|\rho(z=0)|/(2\eta)], \quad \phi_0 = \pi - \arg[\rho(z=0)]. \tag{10}$$

Conservation laws for the NLS system can be expressed either in terms of the potential $q(t, z)$ or in terms of the spectral data. The simplest of the conserved quantities is the L^2-norm of q, the so-called "number of particles." This norm can be written as

$$\int_{-\infty}^{\infty} |q(t, z)|^2\, dt = -\frac{1}{\pi}\int_{-\infty}^{\infty} \ln|a(\xi)|^2\, d\xi + \sum_{k=1}^{N} 2i(\zeta_k^* - \zeta_k), \tag{11}$$

which shows explicitly how the continuous and discrete spectra contribute to the L^2-norm of the potential q. In the following we will often refer to this norm simply as the energy of q, and to the first term on the right-hand side of (11) as the continuous spectrum (or dispersive waves) energy.

In the presence of a general perturbation P, it is not known how to introduce an evolution equation (4) so that the perturbed NLS again arises as the compatibility condition between two linear systems, analogous to equations (3) and (4). Thus, the evolution equation of the spectral data in z cannot be derived, and hence, the solution cannot be reconstructed for $z > 0$. If the perturbation P is small enough, one can find approximate evolution equations for the spectral data via asymptotic expansions. However, these equations will become

invalid after some distance z, typically corresponding to a drastic change in the discrete spectrum when a soliton component vanishes or a new one is generated.

The decomposition into soliton and dispersive components, given by the spectral problem (3), is a valuable alternative to the Fourier transform, because this decomposition provides an efficient way of storing information about the solution. For instance, in the unperturbed case, one soliton mode can replace an infinite number of Fourier components. Moreover, for small perturbations, we can use the decomposition into soliton and dispersive components of the initial condition $q(t, 0)$ and the unperturbed equation to predict the dynamics of the perturbed solution on finite z-intervals. Of course, this is only true for small perturbations P; for large P's there is no a priori argument why the nonlinear Fourier transform should be superior to the linear Fourier transform.

3. NUMERICAL DISCRETIZATION

In this section, we introduce two distinct algorithms for solving the direct Zakharov–Shabat spectral problem. Even though the Zakharov–Shabat spectral problem is defined on the infinite t-line, we have to truncate the potential outside a sufficiently large interval for both algorithms, in order to make its numerical solution possible. As a result, the infinite-line spectral problem is reduced to a problem with a compactly supported potential, and the corresponding boundary conditions can be moved from the $\pm\infty$ to the boundaries of the truncated potential.

The solution of the spectral problem begins by integrating the system of ordinary differential equations (3) with ζ as a complex parameter. The major difference between the two algorithms lies in the way they solve this ODE system. The piecewise-constant approximation utilizes the fact that we can solve the linear ODE system (3) analytically whenever the potential $q(t, z)$ is constant. Since the potential q is discretized on the grid with a time step Δt, one possible approach is to assume that the potential is constant on each subinterval $(t_n - \Delta t/2, t_n + \Delta t/2)$ and solve the direct Zakharov–Shabat problem exactly on each subinterval using matrix exponentials.

It is possible to improve the piecewise-constant algorithm by assuming a higher order approximation for the potential q (i.e., piecewise-linear). In this case one still can solve the ODE system (3) analytically. The disadvantage of this approach is caused by the necessity to use Airy functions in order to express the solution of the ODE system, which leads to a dramatic increase in the computational cost.

High-order numerical integration of the ODE system (3) presents an alternative to the approximate analytical solution. We choose to use the fourth-order Runge–Kutta method [10] as the simplest representative of the high-order ODE solvers.

3.1. *Piecewise-Constant Approximation*

In this subsection we recall the fundamentals of the piecewise-constant approximation for the Zakharov–Shabat spectral problem [3]. The potential $q(t)$ is truncated outside a sufficiently large interval $(-L, L)$. Inside this interval, $q(t)$ is chosen to be equal to a constant $q_n = q(t_n)$ on each elementary subinterval $(t_n - \Delta t/2, t_n + \Delta t/2)$, where the point t_n equals $-L + n\Delta t$. Here, the time step Δt equals $\Delta t = L/M$, with the $2M+1$ being the total number of discretization points of the interval $(-L, L)$. As a result, the corresponding ODE (3) can be solved exactly inside each elementary subinterval for any value of the spectral

parameter ζ. The corresponding solution reads $\mathbf{\Phi}(t_n+\Delta t/2,\zeta)=T(q_n,\zeta)\,\mathbf{\Phi}(t_n-\Delta t/2,\zeta)$, where $\mathbf{\Phi}(t_n-\Delta t/2,\zeta)$ is the "initial" condition on the left end of the elementary subinterval and the transfer matrix $T(q_n,\zeta)$ is the exponential of the matrix $U(q_n,\zeta)$:

$$T(q_n,\zeta)=\exp[-\Delta t U(q_n,\zeta)]=\exp\left[\Delta t\begin{pmatrix}-i\zeta & q_n\\ -q_n^* & i\zeta\end{pmatrix}\right]$$

$$=\begin{pmatrix}\cosh(\kappa\Delta t)-i\zeta\kappa^{-1}\sinh(\kappa\Delta t) & q_n\kappa^{-1}\sinh(\kappa\Delta t)\\ -q_n^*\kappa^{-1}\sinh(\kappa\Delta t) & \cosh(\kappa\Delta t)+i\zeta\kappa^{-1}\sinh(\kappa\Delta t)\end{pmatrix}.$$

The parameter κ, given by the equation $\kappa^2=-|q_n|^2-\zeta^2$, is constant inside each interval Δt.

In order to solve the scattering problem we have to "propagate" the solution using the transfer matrix $T(q_n,\zeta)$ from $-L$ to L. The final result is

$$\mathbf{\Phi}(L-\Delta t/2,\zeta)=\Pi\mathbf{\Phi}(-L-\Delta t/2,\zeta), \tag{12}$$

where

$$\Pi(\zeta)=\prod_{n=1}^{2M}T(q_n,\zeta) \tag{13}$$

is obtained by the ordered multiplication of all transfer matrices. The unknown spectral coefficients $a(\zeta)$ and $b(\zeta)$ can be explicitly expressed in terms of the values of the Jost function $\mathbf{\Phi}_1$ on the "right" end as $t\to\infty$ from (8). By taking the initial condition

$$\mathbf{\Phi}(-L-\Delta t/2,\zeta)=\begin{pmatrix}1\\0\end{pmatrix}e^{i\zeta(L+\Delta t/2)} \tag{14}$$

in Eq. (12), we express the value of the Jost function $\mathbf{\Phi}_1$ on the "right" end in terms of the matrix function Π. On the other hand, we know a priori that this value generates the coefficients a and b,

$$\mathbf{\Phi}_1(L-\Delta t/2,\zeta)=\begin{pmatrix}a(\zeta)e^{i\zeta(-L+\Delta t/2)}\\ b(\zeta)e^{i\zeta(L-\Delta t/2)}\end{pmatrix}$$

and, therefore,

$$\begin{aligned}a(\zeta)&=\Pi_{11}(\zeta)e^{2i\zeta L},\\ b(\zeta)&=\Pi_{21}(\zeta)e^{i\zeta\Delta t}.\end{aligned} \tag{15}$$

To obtain the normalization coefficients ρ_k, we also have to be able to compute the derivative of $a(\zeta)$ with respect to ζ. Differentiation of the expression (15) for $a(\zeta)$ leads to

$$\frac{da}{d\zeta}=2iLa(\zeta)+e^{2i\zeta L}\frac{d}{d\zeta}\big(\Pi_{11}(\zeta)\big). \tag{16}$$

The last term in this expression contains the derivative with respect to ζ of $\Pi_{11}(\zeta)$, the first entry in the matrix from the ordered product (13). Differentiation yields a sum over the partial products that form $\Pi(\zeta)$ times ζ-derivatives of the matrix $T(q_n,\zeta)$. This sum can be computed within the same iteration loop that produces the ordered product Π, with minimal extra cost.

3.2. *Fourth-Order Runge–Kutta Method*

We have also implemented a fourth-order Runge–Kutta algorithm as an alternative to the piecewise-constant approximation. In this case, the matrix $U(q, \zeta)$ serves the role of a known variable coefficient. By switching from the wave function $\mathbf{\Phi} = (\phi_1, \phi_2)^{\mathrm{T}}$ to its envelope $\boldsymbol{\chi} = (\chi_1, \chi_2)^{\mathrm{T}}$,

$$\mathbf{\Phi} = \left(\phi_1 = \chi_1 e^{-i\zeta t}, \phi_2 = \chi_2 e^{i\zeta t}\right)^{\mathrm{T}}, \tag{17}$$

we eliminate the fast oscillations which arise when $\mathrm{Re}(\zeta)$ is large and obtain the following equations for the slowly varying functions $\chi_{1,2}$:

$$\begin{aligned} \frac{d}{dt}\chi_1 &= q\chi_2 e^{2i\zeta t}, \\ \frac{d}{dt}\chi_2 &= -q^*\chi_1 e^{-2i\zeta t}. \end{aligned} \tag{18}$$

The computation of the coefficients a and b via the Runge–Kutta approach is analogous to the same computation via the piecewise-constant approximation. As a result, we need to take special initial conditions at $t = -L$ for $(\chi_1, \chi_2)^{\mathrm{T}} = (1, 0)^{\mathrm{T}}$. Finally, by calculating the value of the vector function χ on the "right" end, we obtain the coefficients a and b as

$$\begin{pmatrix} a(\zeta) \\ b(\zeta) \end{pmatrix} = \begin{pmatrix} \chi_1(L, \zeta) \\ \chi_2(L, \zeta) \end{pmatrix}.$$

To compute the derivative of $a(\zeta)$ obtained with the Runge–Kutta algorithm, we found that an efficient and accurate method is provided by the Romberg algorithm [12].

3.3. *Search for Eigenvalues*

Once we know how to solve the ODE system (3) for any value of the spectral parameter ζ, we can proceed to the solution of the Zakharov–Shabat spectral problem. The numerical computation of the continuous spectrum, defined by the reflection coefficient $r(\zeta) = a(\zeta)/b(\zeta)$ with ζ on the real axis, follows from Eq. (15) or (3.2) in a straightforward fashion. The localization of the discrete eigenvalues ζ_k, located in the upper half of the complex ζ-plane, is not trivial. To find them, we use the facts that the coefficient $a(\zeta)$ can be analytically continued into the upper half ζ-plane from the real axis and that the discrete eigenvalues coincide with the complex zeros of $a(\zeta)$ which we assumed to be simple.

First, following [3], we observe that the total number N of eigenvalues may be computed by calculating the total phase shift of $a(\zeta)$ on the real axis from the "left" end of ζ-axis to the "right": $N = \arg(a(\zeta))|_{-\infty}^{\infty}/(2i\pi)$. Being one-dimensional, this calculation can be performed using a fine ζ grid for maximum accuracy. Second, we implement the grid search for the eigenvalues ζ_k by computing the values of $1/a(\zeta)$ on a sufficiently large grid with preassigned grid size. The grid points at which the value of $1/a(\zeta)$ exceeds a certain practical limit serve as candidates for the eigenvalues. These candidates are tested by trying to further approximate them by using the secant method. Knowledge of the total number N of the discrete eigenvalues indicates whether we have found all of them or not. If we miss some of the eigenvalues, we repeat the search on a refined grid.

We notice that the problem of finding the eigenvalues with small imaginary parts requires special care. This problem is important from a practical point of view because these small eigenvalues may naturally appear during the "birth" or "death" of a soliton. We paid special attention to this problem while implementing the search algorithm.

Another possible approach to the eigenvalue search is to compute a contour integral of the function of a'/a over some closed path in the complex ζ plane. Since $a(\zeta)$ is analytic, this integral will give the number of eigenvalues inside the contour. This technique can be used for both the calculation of the total number of eigenvalues and their localization. We have encountered significant problems during the numerical implementation of this approach. The first problem is caused by the necessity to compute the derivative of $a(\zeta)$. This increases the computation time, in fact drastically so in the case of the Runge–Kutta algorithm. Another, and more serious, limitation of this contour-integral approach is generated by the sensitivity of the above formula when the eigenvalue is located too close to the contour of integration, which requires a rather complicated adaptive algorithm for selecting the path of integration.

4. ERROR ESTIMATES

4.1. *Error for Piecewise-Constant Approximation*

To estimate the numerical error for the piecewise-constant approximation, one can use perturbation results obtained for the Zakharov–Shabat spectral problem (see, e.g., [13]). According to this approach, the piecewise-constant approximate potential q_{pwc} is nothing but the perturbed exact potential: $q_{\text{pwc}} = q + \delta q$. The error in the coefficient $a(\zeta)$ is expressed in terms of an integral over the perturbation δq of the potential, and the functions $\phi_{1,2}$ and $\psi_{1,2}$ which are components of the corresponding unperturbed Jost vector functions $\mathbf{\Phi}_1$ (5) and $\mathbf{\Psi}_2$ (6):

$$\delta a = \int_{-\infty}^{\infty} dt\,(\delta q \phi_1 \psi_1 + \delta q^* \phi_2 \psi_2). \tag{19}$$

For the purposes of the error analysis it is sufficient to consider only the first term in the expression (19). The second term can be estimated in a similar fashion. Using the shorthand notation $f = \phi_1 \psi_1$, we can rewrite the error caused by the first term as $\int_{-\infty}^{\infty} \delta q f\, dt$.

To estimate the error contribution $\Delta a = \int_{-\Delta t/2}^{\Delta t/2} \delta q f\, dt$ added on the elementary subinterval $(-\Delta t/2, \Delta t/2)$, we represent δq as $\delta q = q(t) - q(0)$ and expand f and q in Taylor series. As a result, we obtain

$$\Delta a = \left(\frac{\Delta t}{2}\right)^3 \frac{1}{3}[f q'' + 2 f' q'] + O((\Delta t)^4), \tag{20}$$

where $' = d/dt$. The fact that we choose the grid point in the middle of the elementary subinterval is essential for obtaining $(\Delta t)^3$—dependence for the local error Δa. By summing up the local errors Δa over the whole interval $(-L, L)$ we obtain that the global error in $a(\zeta)$ is proportional to $(\Delta t)^2$.

The complex spectral parameter ζ so far has been hidden in the error estimate for a, which is valid for any value of ζ. To analyze the ζ-dependence of the error δa, we need to

look at the expression (20) more closely. By using the asymptotic expression for the vector Jost functions at large ζ,

$$\mathbf{\Phi}_1 \sim \begin{pmatrix} 1 \\ 0 \end{pmatrix} \exp(-i\zeta t)[1 + o(1)], \quad \zeta \to \infty, \tag{21}$$

$$\mathbf{\Psi}_2 \sim \begin{pmatrix} 0 \\ 1 \end{pmatrix} \exp(i\zeta t)[1 + o(1)], \qquad \zeta \to \infty, \tag{22}$$

we obtain $f, df/dt \sim \zeta^{-1}$. Thus, at large values of ζ

$$\delta a \sim \frac{\Delta t^2}{\zeta}.$$

Therefore, the global numerical error in the coefficient $a(\zeta)$ decreases with ζ which is in contrast with the case for the Runge-Kutta case presented below, where the corresponding error increases beyond all bounds as $\zeta \to \infty$.

The second-order global numerical error for the coefficient $a(\zeta)$ translates into an error of the same order for the eigenvalues ζ_k. An additional source of error during the numerical computation of the eigenvalues ζ_k is created by the iteration process in the secant method. This additional error is controlled by finding the zeros of a with high precision. Therefore, the total error in the eigenvalues is kept at second order in Δt.

The numerical error for the coefficient b is estimated in a similar way. It is also of second order in Δt.

4.2. *Error for Runge–Kutta Method*

An estimate of the local truncation error for the Runge–Kutta method can be found in a standard fashion [10, 11]. The exact solution $\mathbf{\Phi} = (\phi_1, \phi_2)^{\mathrm{T}}$ satisfies system (2).

The approximate solution $\mathbf{\Phi}_n^{(a)} = (\phi_{1_n}^{(a)}, \phi_{2_n}^{(a)})^{\mathrm{T}}$, $n = 0, 1, 2, \ldots$, satisfies the difference equation (DE)

$$\mathbf{\Phi}_{n+1}^{(a)} = \mathbf{\Phi}_n^{(a)} + \Delta t \boldsymbol{G}\big(\mathbf{\Phi}_n^{(a)}, q; \zeta\big), \tag{23}$$

with the function $\boldsymbol{G}(\mathbf{\Phi}_n^{(a)}, q; \zeta)$ given by

$$\boldsymbol{G}\big(\mathbf{\Phi}_n^{(a)}, q; \zeta\big) = \frac{1}{6}(\boldsymbol{k}_1 + 2\boldsymbol{k}_2 + 2\boldsymbol{k}_3 + \boldsymbol{k}_4),$$

where the $\boldsymbol{k}$'s are given by the usual Runge–Kutta iterations of the (linear) function $\boldsymbol{F}(\mathbf{\Phi}, q; \zeta)$ at the right-hand side of system (2), starting with $\boldsymbol{k}_1 = \boldsymbol{F}(\mathbf{\Phi}, q; \zeta)$. The local truncation error,

$$\boldsymbol{\tau}(t_0) \equiv \frac{\mathbf{\Phi}(t_0 + \Delta t) - \mathbf{\Phi}(t_0)}{\Delta t} - \boldsymbol{G}(\mathbf{\Phi}(t_0), q(t_0); \zeta)$$

on the elementary subinterval $t \in (t_0, t_0 + \Delta t)$, has a standard representation

$$\boldsymbol{\tau} = C\boldsymbol{F}^{(IV)} \cdot (\Delta t)^4, \quad \boldsymbol{F}^{(IV)} = \frac{d^4}{dt^4}\boldsymbol{F}\bigg|_{t=t_0+\theta 2\Delta t}, \quad 0 < \theta < 1. \tag{24}$$

From Eq. (23) (see [11]) it follows that the global discretization error $|\mathbf{\Phi}(t_n) - \mathbf{\Phi}_n^{(a)}| \sim \tau$. Also, by differentiating the function $\boldsymbol{F}$ as in formula (24) four times, we derive that the local truncation error has a fifth-order dependence on ζ: $\tau \sim \zeta^5$ due to the presence of the terms $i\zeta\phi_1$ and $i\zeta\phi_2$ in $\boldsymbol{F}$. Moreover, this fifth-order dependence accumulates even in regions where the potential q is identically zero.

To improve the accuracy of the Runge–Kutta approach, we make the change of variables (17) by switching from the wave function itself to its envelope χ. As a result, the transformed right-hand side of Eq. (18) no longer has a term linear in ζ, and the oscillatory term $\exp(2i\zeta t)$ is restricted to the support of the potential q. Therefore, the local truncation error τ for the Runge–Kutta discretization of Eq. (18) is proportional to the fourth power of ζ. Moreover, the proportionality coefficient is nonzero only on the support of q.

Note that the local truncation error τ causes corresponding errors for all the computed spectral characteristics, such as the discrete eigenvalues and the continuous spectrum (see Fig. 1 and the tables in Section 5).

We will test these error estimates in the next section. For noncompact support potentials q we always use a sufficiently large interval $(-L, L)$, so that the error generated by neglecting the potential outside this finite domain is negligible, compared with the local error of any of the two integration methods.

5. TESTS

We have implemented both the piecewise-constant approximation and the fourth-order Runge–Kutta algorithms in Fortran 77. We have performed a series of tests on a Silicon Graphics workstation under the operating system IRIX64 release 6.1 with the R8000 75 MHz processor. All computations were done in double precision. To illustrate the performance of the program we present the CPU time for the one-soliton potential. The CPU time depends on a variety of parameters: on the number of points used for the discretization, on the number of discrete eigenvalues, and their position in the complex ζ-plane.

5.1. *One-Soliton Potential*

First, we consider the simplest possible case, namely, a one-soliton potential (10), whose spectrum is known exactly. We have chosen the soliton parameters so that the corresponding eigenvalue ζ equals $\frac{1}{2}(1+i)$ and the normalization coefficient b/a' equals $-i$. As a result, the one-soliton potential equals $q(t) = \exp(-it)/\cosh(t)$. For the "pure" soliton potential, there is no continuous spectrum.

The numerical results for this soliton potential, presented in Tables I and II, demonstrate that for this particular case all the spectral data (the discrete eigenvalue, the normalization coefficient, and the continuous spectrum) are found with good accuracy. The "Cont. Sp. En." column in Table I denotes the numerical value of the continuous spectrum (dispersive waves) contribution to the L^2-norm of q, calculated from formula (11). Figure 1 shows that our implementations of the Runge–Kutta and piecewise-constant approximation methods are of fourth order and second order in time step, respectively. This result agrees with the analytical error estimates derived in Section 4.

Note that Table II, unlike Table I, does not have the "Continuous Spectrum Energy" column. The reason for this is that the Runge–Kutta method produces an error of order one when it calculates this parameter.

TABLE I
The Spectrum of a One-Soliton Potential Obtained by Using the Piecewise-Constant Algorithm

Points	Δt	Discr. Eigenvalue	Cont. Sp. En.	Norm. Coeff.
128	0.3125	$0.49725 + i0.49460$	1.7E-02	$1.2E\text{-}04 - i0.98927$
256	0.1562	$0.49931 + i0.49864$	3.3E-03	$5.4E\text{-}06 - i0.99728$
512	0.0781	$0.49983 + i0.49966$	1.2E-07	$1.9E\text{-}06 - i0.99931$
1024	0.0391	$0.49995 + i0.49991$	7.9E-09	$-5.6E\text{-}07 - i0.99982$
2048	0.0195	$0.49998 + i0.49997$	4.9E-10	$-3.9E\text{-}06 - i0.99994$
Exact		$0.5 + i0.5$	0	$-i$

We also provide a comparison of the CPU time that each algorithm takes to complete the task of finding the one-soliton spectrum of Tables I and II. The Runge–Kutta-based algorithm is roughly 20–30% faster than the piecewise-constant method for this particular task. In general, over all the tests we have conducted, the two algorithms' speeds were roughly the same. Of course, the running time for both algorithms is architecture-dependent and the CPU times we present (obtained on the IRIX workstation) are meant to give the reader an idea about the cost of the computations in this particular case (see Table III). The two algorithms share the same routines for the eigenvalue search in the complex plane, and in both cases most of the CPU time is spent by the procedure which locates the discrete eigenvalues in the complex ζ plane. In particular, in the test for one-soliton potential both algorithms spend over 80% of their time searching for the zero of $a(\zeta)$. The majority of time during the search is spent on computing the values of $a(\zeta)$ on the grid.

We stress that the time for locating the eigenvalues depends considerably on their position in the complex ζ plane. We implemented an algorithm which starts the search for the eigenvalues from the imaginary axis and then propagates to the left and to the right simultaneously. Therefore, the time spent for locating the eigenvalues is proportional to amplitudes of their real parts. The coefficient of proportionality depends on the grid spacing and the number of nodes in the grid.

5.2. *Oversoliton*

Our next test aims at checking how accurately both the piecewise-constant and Runge–Kutta approaches calculate a nonzero continuous spectrum. As a test potential we take

TABLE II
The Spectrum of a One-Soliton Potential, Obtained by Using the Fourth-Order Runge–Kutta Approach

Points	Δt	Discr. Eigenvalue	Norm. Coeff.
128	0.3125	$0.499999990 + i0.499270300$	$7.60E\text{-}08 - i0.99746220$
256	0.1562	$0.499999990 + i0.499949000$	$8.32E\text{-}08 - i0.99984100$
512	0.0781	$0.499999990 + i0.499996700$	$8.38E\text{-}08 - i0.99999000$
1024	0.0391	$0.499999990 + i0.499999790$	$8.39E\text{-}08 - i0.99999930$
2048	0.0195	$0.499999997 + i0.499999987$	$8.39E\text{-}08 - i0.99999996$
Exact		$0.5 + i0.5$	$-i$

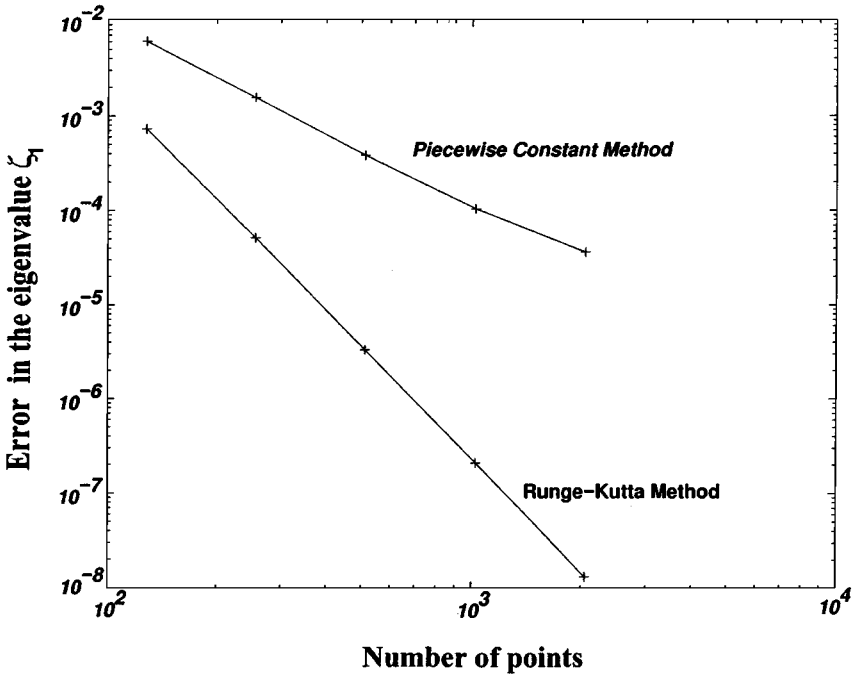

FIG. 1. Error in the eigenvalue ζ_1 versus the number of discretization points for one-soliton potential (see Tables I and II).

$q(t) = 2A\exp(-0.3t)/\cosh(2t)$ (so-called oversoliton) where the parameter A must be chosen to be 1 for a "pure" soliton, but in our case A may have any positive value. For such a potential, the Zakharov–Shabat scattering problem can be solved analytically for any value of A [14]. In general, both the discrete and continuous spectra are present in the problem. In the case when $A = 1.4$, there is a single eigenvalue $\zeta_1 = 0.15 + 1.8i$, plus a certain amount of nonzero continuous spectrum. We choose not to present the lengthy expressions for the coefficients $a(\zeta)$ and $b(\zeta)$ (see [14]). Out of the total pulse energy $E_{\text{total}} = 4A^2 = 7.84$, the soliton part is $E_{\text{sol}} = 4\eta = 7.2$, while the rest of the energy is contained in the nonsoliton component: $E_{\text{cont.spectr.}} = 0.64$.

Tables IV and V contain the numerical results on the discrete spectrum plus the pulse energy due to the nonsoliton component and illustrate that, with respect to the calculation of the continuous spectrum, the piecewise-constant approach is by far superior to the Runge–Kutta method.

TABLE III
CPU Time of Computations

Points	Piecewise-constant	Runge–Kutta
128	67 s	51 s
256	135 s	102 s
512	275 s	205 s
1024	573 s	409 s
2048	1236 s	816 s

TABLE IV

Spectrum of the Oversoliton Potential: $q(t) = 2A\exp(-0.3t)/\cosh(2t)$ with $A = 1.4$, Obtained by Using a Piecewise-Constant Approximation

Points	Δt	Discr. eigenvalue	Cont. Sp. En.
128	0.3125	$0.146174 + i1.778069$	0.7126577
256	0.1562	$0.149087 + i1.794385$	0.6536514
512	0.0781	$0.149774 + i1.798589$	0.6399762
1024	0.0391	$0.149943 + i1.799647$	0.6399930
2048	0.0195	$0.149985 + i1.799911$	0.6399987
Exact		$0.15 + i1.8$	0.64

In Table V we do not present data on the continuous spectrum energy because in all cases, except the case of 2048 points ($\Delta t = 0.0195$), the Runge–Kutta method produces errors of order 1.

5.3. *Rectangular Potential*

In the final test, we analyze the integrators' performance in the case of discontinuous potentials. We consider the rectangular potential $q(x) = q_0$, $|x| < L$. For such a potential, explicit formulas exist for the coefficients a and b, which are

$$a(\zeta) = e^{2i\zeta L}\left[\cos(2\nu L) - \frac{i\zeta}{\nu}\sin(2\nu L)\right], \quad b(\zeta) = -\frac{q_0}{\nu}\sin(2\nu L),$$

where the parameter ν is expressed in terms of the spectral parameter ζ and the potential amplitude q_0 in the form $\nu^2 = \zeta^2 + q_0^2$. In our test, we have chosen the following values for the potential amplitude q_0 and the potential width L: $q_0 = -\pi/2$, $L = 1$. The total energy in this case is $\pi^2/2$. To determine the eigenvalues, one has to look for the zeros of the coefficient $a(\zeta)$. As a result, one determines that the rectangular potential with the given choice of parameters leads to a single purely imaginary discrete eigenvalue $\zeta_1 \approx 1.062572i$. Hence, the energy of the continuous spectrum is $E_{\text{cont.spec.}} \approx 0.6845133$. The main difference between this and the previous tests is that the potential is not smooth, which leads to larger errors for both the piecewise-constant and Runge–Kutta methods. Notice that in the case of the piecewise-constant method this error is caused solely by the need to

TABLE V

Spectrum of the oversoliton potential: $q(t) = 2A\exp(-0.3t)/\cosh(2t)$ with $A = 1.4$, Obtained by Using the Fourth-Order Runge–Kutta Approach

Points	Δt	Discr. eigenvalue
256	0.1562	$0.14999998 + i1.790426$
512	0.0781	$0.14999998 + i1.799356$
1024	0.0391	$0.14999997 + i1.799959$
2048	0.0195	$0.14999997 + i1.799997$
Exact		$0.15 + i1.8$

TABLE VI
Comparative Performance of Both the Piecewise-Constant Approximation and the Fourth-Order Runge–Kutta Method

Points	Δt	Piecewise-Const. method	Runge–Kutta method
128	0.3125	0.12205	0.46012
256	0.1562	0.01897	0.19840
512	0.0781	0.02746	0.20978
1024	0.0391	0.00467	0.04209
2048	0.0195	0.00707	0.01101

Note. The maximum error in the energy density of the continuous spectrum for the rectangular potential.

evaluate the potential at the middle of the discretization step; with the proper discretization the piecewise-constant algorithm naturally yields an exact solution for the rectangular potential.

The continuous spectrum energy is nonzero for the rectangular potential. In this test we analyze not only the numerical errors incurred in the calculation of the integral characteristic, such as the total energy input by the continuous spectrum, but also the numerical errors in the local characteristic—a measure of the intensity of the dispersive waves, $\sup_\zeta |(2/\pi)\log|a(\zeta)||$, where ζ is on the real axis.

As expected, we can see that the piecewise-constant approximation performs much better, compared with the results of the fourth-order Runge-Kutta method (Table VI).

Finally, we present the numerical results for the full spectral data of the rectangular potential (Tables VII and VIII).

The Runge–Kutta method computes the continuous radiation correctly only for $\Delta t = 0.01953125$ (2048 points). In all other cases, this method produces an error of order one. Moreover, the Runge–Kutta method completely fails for $\Delta t = 0.3125$—the method in this case gives the wrong number of eigenvalues.

Our numerical results demonstrate that in the case of a rectangular potential, the convergence of all the spectral parameters is much slower, compared with the two previous tests. This is due to the discontinuity of the rectangular potential, which results in the fact that the error estimates involving the derivatives of the potential, which we derived in the previous section, are not quite valid.

TABLE VII
Spectrum of the Rectangular Potential Obtained by Using the Piecewise-Constant Approximation

Points	Δt	Discr. eigenvalue	Cont. Sp. En.	Norm. Coeff.
128	0.3125	2.1E-09 + i1.13409	0.836357	2.7E-08 + i2.85167
256	0.1562	2.4E-09 + i1.07568	0.684812	2.1E-08 + i2.39278
512	0.0781	1.6E-09 + i1.04187	0.627221	1.1E-08 + i2.23392
1024	0.0391	5.8E-09 + i1.05920	0.653978	4.5E-08 + i2.27612
2048	0.0195	1.2E-09 + i1.06755	0.668988	1.0E-08 + i2.30095
Exact		i1.062572	0.6845133	i2.283050

TABLE VIII
Spectrum of the Rectangular Potential Obtained by Using the Fourth-Order Runge–Kutta Approach

Points	Δt	Discr. eigenvalue	Norm. Coeff.
128	0.3125		
256	0.1562	4.68E-09 + i1.055425	3.57E-08 + i2.266125
512	0.0781	5.37E-10 + i1.030430	3.75E-09 + i2.186588
1024	0.0391	1.02E-09 + i1.064940	8.11E-09 + i2.291327
2048	0.0195	1.62E-09 + i1.070325	1.32E-08 + i2.309555
Exact		i1.062572	i2.283050

We also remark that in our tests for the one-soliton potential and oversoliton, the Runge–Kutta algorithm finds the discrete spectrum eigenvalues with higher accuracy than the piecewise-constant approximation. This is in accordance with our error analysis, since the tests' eigenvalues are within or close to the unit circle (cf. Tables I and II, IV and V). Because of the discontinuity in the potential, this advantage of the Runge–Kutta method is lost in the case of the rectangular potential (cf. Tables VII and VIII).

The results obtained in this section prove that, overall, the piecewise-constant approximation is superior to the fourth-order Runge–Kutta method as a tool for finding the Zakharov–Shabat spectrum of the solutions to the NLS equation.

6. NON-RETURN-TO-ZERO TO SOLITON DATA CONVERSION PROBLEM

In this section, we illustrate the performance of our code utilizing the piecewise-constant approximation on a light pulse propagation problem in nonlinear optical fibers.

A very simple and effective source of solution-like pulses in optical soliton transmission experiments was proposed and implemented recently [8]. The basic idea is to generate a soliton signal starting from a Non-return-to-zero (NRZ) source and imposing a subsequent sinusoidal phase modulation of each NRZ bit, where the modulation frequency is chosen to be equal to the bit rate. If this signal is injected into a transmission line with sliding-frequency guiding filters then, after a complicated transient evolution, localized soliton-like pulses emerge (see Fig. 2, where for simplicity we consider the case of one single bit). Therefore, this phenomenon can be used to implement a method of converting NRZ bit streams into soliton signals. We consider an optical transmission line with periodically spaced, lumped amplifiers, each followed by a Fabry–Perot filter whose peak frequencies are shifting ("sliding") linearly with the distance along the line. When the dispersion length is much larger than the amplifier spacing, a good model for signal transmission is the "averaged," normalized, NLS (1)
[4, 15, 16] with the following perturbation P:

$$P = (i/2)\left[\alpha q - \beta(i\partial_t - \omega_f)^2 q\right]. \tag{25}$$

This perturbation models the Fabry–Perot filter via the "Gaussian" approximation, which is defined by three main parameters: β is the filter strength, α is the excess gain, while ω'_f

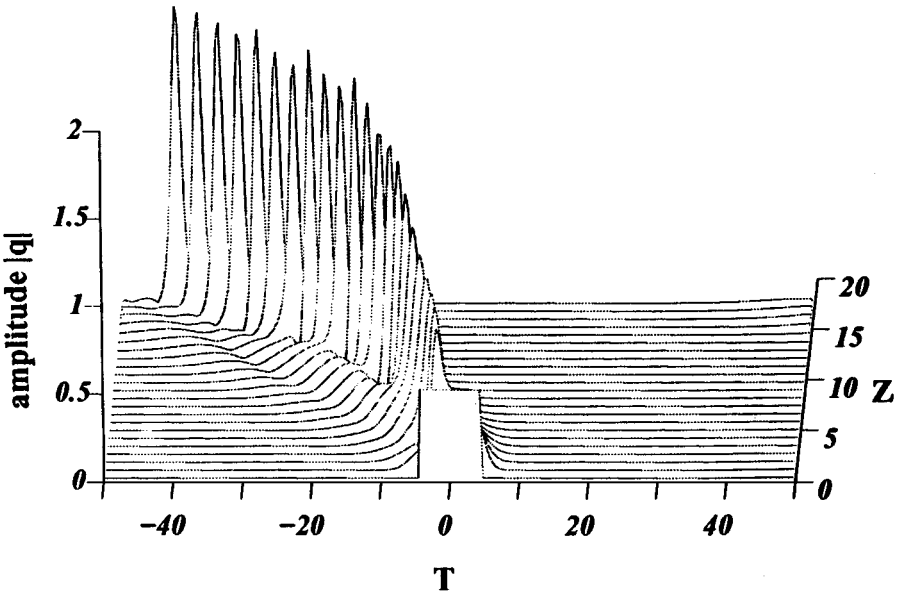

FIG. 2. Conversion of a single NRZ-phase-modulated bit into a soliton in a transmission line with sliding-frequency guiding filters (numerical simulation).

parameterizes the sliding rate of the peak frequency of the filters, ω_f, with the distance,

$$\omega_f = \omega_0 + \omega_f' z, \tag{26}$$

where ω_0 denotes the initial filter frequency offset from the carrier.

The initial condition for Eqs. (1), (25), which we focus on, is the phase-modulated NRZ signal

$$q_0(t) = a(t) \exp[i\mu \sin(\Omega t)], \tag{27}$$

where $a(t)$ is the NRZ signal flipping between 0 and A. We have used the following practical normalized values of the system parameters for the present problem $\alpha = 0.4$, $\beta = 0.4$, $\omega_f' = 0.185$, $\Omega = 2\pi/8.82$. The amplitude A and the depth of phase modulation μ then can serve as the optimization parameters for the converted soliton-like pulse.

By applying our code to the initial pulse with the amplitude A and the depth of phase modulation μ chosen equal to 1 and 0.7π, respectively, we can clearly see that it is equivalent to four soliton eigenvalues: $\zeta_1 = 0.57 + 0.79i$, $\zeta_2 = -0.56 + 0.15i$, $\zeta_3 = -0.36 + 0.55i$, $\zeta_4 = -0.1 + 0.54i$, plus a small amount of dispersive waves (about 10% in terms of the total pulse energy). Thus, the initial pulse consists of the primary soliton eigenvalue $\zeta_1 = 0.57 + 0.79i$ (the initial filter position coincides with the primary eigenvalue frequency: $\xi_1 = \mathrm{Re}(\zeta_1)$), which gives rise to the output soliton, plus extra modes which are suppressed by the in-line filtering. Notice that while they are present, these additional components act like noise in the system and can lead to signal corruption by an uncontrollable shift of the position of the primary soliton in its time slot. To provide an efficient conversion of the phase-modulated NRZ signal into solitons, it is therefore important to suppress this noise as early as possible during the transmission. A hybrid numerical–analytical approach was proposed in [9] to analyze the conversion of an NRZ input to a soliton output signal in

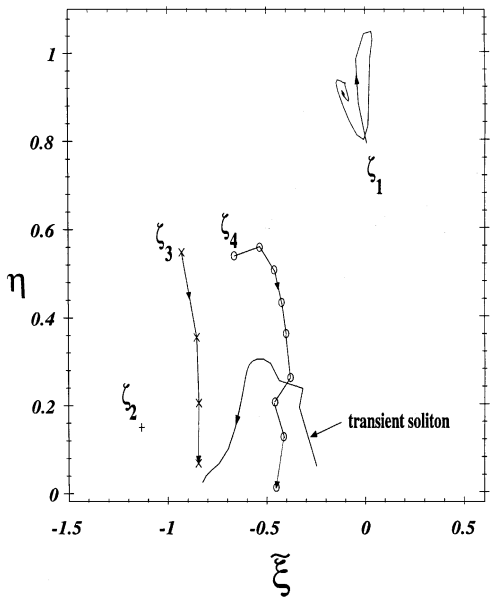

FIG. 3. The trajectories of all eigenvalues detected in the initial condition (27) (based on the numerical simulation of the full equation processed by the nonlinear spectral transform). Here, $\tilde{\xi}$ is the eigenvalue frequency with the sliding part being subtracted: $\tilde{\xi} = \xi - \omega_f' z$.

an optical line with sliding frequency guiding filters. The numerical part consists of applying the nonlinear spectral transform solver to the input signal. This allows us to identify the soliton modes in the signal and then to follow the evolution of each single soliton mode by applying the adiabatic approximation.

Another possible approach is to compute the solution of the perturbed nonlinear Schrödinger equation (1) numerically with the NRZ signal as an initial condition and then to analyze snapshots of the solution using the spectral code to provide a clear picture of how the spectral data evolves in time. We illustrate the application of this approach to the example above. Figure 3 presents the time evolution of the eigenvalues under the filtering perturbation (25). Only one (primary soliton) out of four survives. Here, $\tilde{\xi}$ is the eigenvalue frequency with the sliding part being subtracted: $\tilde{\xi} = \xi - \omega_f' z$. Note that our code is sensitive enough to catch the emergence of a transient soliton, which was absent at the beginning. In the unperturbed case, soliton and nonsoliton modes do not interact with each other, but this is not so in the general perturbed case. When one of the secondary solitons disappears, it leaves behind a packet of dispersive waves. This wave packet can in turn start to accumulate enough energy which it eventually "sheds" in the form of a small-amplitude transient soliton.

It is remarkable that, with the exception of these transient episodes, the results on the time evolution of the eigenvalues obtained numerically with the help of the nonlinear spectral transform are in good agreement with the the results predicted by the adiabatic approximation. In fact, the availability of the nonlinear spectral code in this problem ultimately verifies (and extensively complements) the adiabatic approximation. Such a code helps in answering basic questions, such as: "How close is the output pulse to a soliton of the unperturbed NLS?" We calculate the amount of energy of the dispersive waves contained in the output pulse by using our code and can definitely say that for the given practical parameters,

the output pulse is an almost "pure" soliton. Only 2% of the total pulse energy is in the nonsoliton components when the conversion process is over.

7. CONCLUSIONS

In this work, we have implemented two different algorithms to compute numerically the direct spectral transform (the direct Zakharov–Shabat eigenvalue problem on the infinite line) which is used heavily in soliton theory and its applications in nonlinear fiber optics. The first algorithm uses a piecewise-constant approximation to the potential in order to solve the corresponding ODE, and the second algorithm uses the fourth-order Runge–Kutta method.

We have tested and compared the performance of these two algorithms on three exactly solvable potentials. We find that, despite the fact that the truncation error of the Runge–Kutta method is of higher order, the additional dependence of this error on the eigenvalues of the Zakharov–Shabat spectral problem limits the usefulness of the Runge–Kutta approach. Ultimately, this method can be effective only within the unit disk around the origin of the complex plane of the eigenvalues. This is a critical limitation when computing the nonsoliton part of the nonlinear spectrum, which can receive significant contributions from intervals along the real axis far from the origin. Moreover, this additional dependence poses restrictions on the class of potentials for which the discrete soliton spectrum can be computed accurately. One example, which is important for signal analysis via nonlinear Fourier transform, is that of a potential $q(t)$ which varies slowly in t (and so the length $2L$ for the ODE computation can be fairly large). From system (2), it is easy to show through a simple rescaling of time that this case is equivalent to one with a large amplitude potential and a (rescaled) large eigenvalue parameter $|\zeta|$. Thus, based on our error analysis, the Runge–Kutta method can be expected to lose accuracy in this case.

The limitation suffered by the Runge–Kutta method can be expected to affect any high-order ODE integrator. It is directly caused by the fact that the numerical truncation error of the nth order method is proportional to the nth time derivative of the right-hand side of the spectral ODE, $\boldsymbol{F}^{(n)}(\Delta t)^n$, where $\boldsymbol{F}$ is the right-hand side of the ODE (18), and Δt is the mesh size. Due to the presence of the spectral parameter ζ in the ODE, one has $|\boldsymbol{F}^{(n)}| \sim \zeta^n$, or ζ^{n+1}, depending on which Eq. (18) or (3) is used. Therefore, any attempt to increase the accuracy of the numerical solution by using a higher order numerical integrator automatically fails as soon as $|\zeta| \gg 1$. We have found that no such limitations exist for the piecewise-constant approximation, and in fact, the truncation error for this method *decreases*, instead of increasing, with large $|\zeta|$ as $|\zeta|^{-1}$. Conversely, the truncation error analysis for higher order methods points to the fact that an efficient search for eigenvalues near the origin is most effectively carried out using a higher order method like Runge–Kutta.

In summary, our work shows that the piecewise-constant approximation algorithm is the better tool overall; it is the most robust and offers the same efficiency for the computation of both discrete and continuous spectra.

We have illustrated the performance of a code based on this algorithm by applying it to NRZ-to-soliton data conversion problem in a fiber-optical line with sliding frequency-guiding filters. One of the important features of our algorithm is the optimization of the search for eigenvalues in case of multiple snapshots of the potential. The NRZ-to-soliton data conversion problem provides an example where the flow of the spectral data in perturbed integrable systems needs to be analyzed. This problem can be divided into two independent

tasks. First, the numerical solution of the perturbed equation is computed on a time grid of stepsize δt. Second, a spectral code is utilized to analyze snapshots of the numerical solution taken at times δt apart. We make use of the fact that in most cases the spectral data are order δt close for two consecutive snapshots of the numerical solution, and therefore it is possible to use the spectral data computed for one snapshot of the potential as the initial guess for the spectral data of the next snapshot. This optimization of the search algorithm makes a tremendous difference when there are eigenvalues with large (in absolute value) real parts. For example, we found that if there are eigenvalues with real parts greater than 0.5 then the search is more than five times faster if the information from the previous snapshot of the potential is used. The optimized code is therefore especially valuable for tracking the eigenvalues of potentials obtained as numerical simulations of perturbed integrable equations.

ACKNOWLEDGMENTS

The authors thank A. R. Osborne for his numerous stimulating remarks and E. A. Overman for helpful discussion. S. Burtsev and R. Camassa acknowledge support from the U.S. Department of Energy under Contract W-7405-ENG-36 and the Applied Mathematical Sciences Contract KC-07-01-01. I. Timofeyev thanks the Theoretical Division and Center for Nonlinear Studies at the Los Alamos National Laboratory for their hospitality and support during the summers of 1995 and 1996 and acknowledges support from the U.S. Department of Energy under Contract DE-FG02-93ER25154 and the National Science Foundation through the NSF Traineeship DMS-9256302 and Grants DMS-9502142 and DMS-9510728.

REFERENCES

1. S. V. Manakov, S. P. Novikov, L. P. Pitaevskii, and V. E. Zakharov, *Theory of Solitons* (Consultants Bureau, New York, 1984).
2. M. J. Ablowitz and H. Segur, *Solitons and the Inverse Scattering Transform* (SIAM, Philadelphia, 1981).
3. G. Boffetta and A. R. Osborne, Computation of the direct scattering transform for the nonlinear Schrödinger equation, *J. Comput. Phys.* **102**, 252 (1992).
4. A. Hasegawa and Y. Kodama, *Solitons in Optical Communication* (Oxford Univ. Press, Oxford, 1995).
5. G. P. Agrawal, *Nonlinear Fiber Optics*, 2nd ed. (Academic Press, San Diego, 1994).
6. V. E. Zakharov and A. B. Shabat, *Sov. Phys. JETP* **34**, 62 (1972).
7. A. R. Bishop, M. G. Forest, D. W. McLaughlin, and E. A. Overman II, A quasiperiodic route to chaos in a near-integrable PDE. Spatio-temporal coherence and chaos in physical systems, *Phys. D* **23** (1–3), 293 (1986).
8. P. V. Mamyshev and L. F. Mollenauer, *OFC'95 Technical Digest*, 302 (1995).
9. S. Burtsev, R. Camassa, and P. Mamyshev, *The NRZ-to-Soliton Data Conversion Problem*, Los Alamos National Lab Report LAUR 97-347 (1997).
10. W. H. Press, S. A. Teukolsky, W. T. Vetterling, and B. P. Flannery, *Numerical Recipes*, 2nd ed. (Cambridge Univ. Press, New York, 1992).
11. J. Stoer and R. Bulirsch, *Introduction to Numerical Analysis* (Springer-Verlag, New York/Berlin, 1991).
12. G. Engeln-Mullges and F. Uhlig, *Numerical Algorithms with C* (Springer-Verlag, New York/Berlin, 1996).
13. A. C. Newell, The inverse scattering transform, in *Solitons*, edited by R. K. Bullough and P. J. Caudrey (Spriner-Verlag, New York/Berlin, 1980).
14. J. Satsuma and N. Yajima, Initial value problem in one-dimensional self-modulation of nonlinear waves in dispersive media, *Progr. Theor. Phys.* **55**, 284 (1974).
15. L. F. Mollenauer, J. P. Gordon, and S. G. Evangelides, The sliding-frequency guiding filter: An improved form of soliton jitter control, *Opt. Lett.* **17**, 1575 (1992).
16. A. Hasegawa and Y. Kodama, Guiding-center soliton in optical fibers, *Opt. Lett.* **15**, 443 (1990). [Guiding-center soliton, *Phys. Rev. Lett.* **66**, 161 (1991)]